Journal of Hazardous Materials, 15 (1987) 377–417
Elsevier Science Publishers B.V., Amsterdam — Printed in The Netherlands

VALIDATION OF FLUID MODELING TECHNIQUES FOR ASSESSING HAZARDS OF DENSE GAS CLOUD DISPERSION

ROBERT N. MERONEY

Fluid Mechanics and Wind Engineering Program, Civil Engineering Department, Colorado State University, Fort Collins, CO 80523 (U.S.A.)

(Receive May 3, 1986; accepted in revised form November 11, 1986)

Summary

Data from twenty six dense gas field experiments are compared with physical model simulations. In general the model clouds are very similar in appearance, they spread and travel at correct rates, measured concentrations compare very well, and peak concentrations are often predicted to within a factor of two or better. Model simulations where specific gravity, volume flux ratio and Froude number equality are maintained produce the most successful predictions of field concentrations. When only volume flux ratio and flux Froude number equality are stipulated, peak concentration isopleths are preserved, but the time of arrival and departure of the dense clouds are distorted. Field/fluid model comparisons reveal that lower flammability distances for liquified natural gas or propane spills are predicted within a standard deviation of +25% with a 90% level of confidence.

1.0. Introduction

It is important that accurate predictive models for flammable or toxic vapor cloud behavior be developed, so that the associated hazards of transportation and storage may be realistically assessed. Thermal effects, topography, the presence of obstacles and spray curtain mitigation devices can affect the dispersion of dense gas clouds. Fluid or physical modeling studies are often desirable because such variables can be controlled at will, with great savings in time and expense over full-scale tests. The physical model inherently includes fluid physics for which only limited understanding can presently be incorporated in numerical models.

However, certain constraints exist on a physical model's ability to predict plume behavior. These constraints are due to the limited range of transport properties of air and water, the inherent characteristics of fluid turbulence, and the size range of available fluid modeling facilities. The primary intent of this paper is to review those model experiments which were performed to simulate well-documented field experiments, and assess the capabilities and lim-

0304-3894/87/$03.50

itations of physical modeling techniques. Such a verification exercise is appropriate if physical modeling is to be a credible predictive approach.

A single field event has a large number of additional uncontrolled or poorly specified variables which have an effect on the resultant concentration field that are not completely accounted for by either a physical or numerical modeling. The source conditions of a cryogenic spill situation must be approximated, because it is difficult to predict or measure the time-dependent source size and boiloff characteristics accurately in the field. The wind field into which a dense plume is released is typically nonstationary. The plume may experience a wind field that is undergoing a change of mean wind speed, mean wind direction, and turbulent characteristics with time. In wind tunnel or water channel simulations the wind characteristics are assumed to be constant, i.e., statistically stationary. These assumptions may lead to differences between the resultant concentration fields depending on the severity of the nonstationarities during the field tests.

A top priority during evaluation is to determine how accurate physical modeling may be under realistic conditions. One desires to reasonably represent the spatial and temporal distribution of the plume concentration. For liquefied natural gas (LNG) or liquefied petroleum gas (LPG) hazard evaluation the spatial distribution of plume concentrations appears to be more critical than the temporal distribution. A pattern comparability test is described in Section 2.0 that provides a quantitative measurement of how well the modeled spatial distribution of ground-level concentration agrees with real field observations.

Other verification criteria include the decay rate of peak concentrations with distance, distances to lower flammability limit (LFL), general plume appearance, overlays of peak concentration isopleths, and overlays of concentration time histories at measurement locations.

2.0. Surface pattern comparability approach

Most model performance measures compare predicted versus observed values directly. Precise pairing in time and space imposes too strong a penalty on small misalignments, while pairing in time alone provides no information on spatial variability. Lewellen and Sykes [1] have proposed a novel measure of spatial comparison between observed and calculated patterns which compares over increments of decreasing spatial resolution. Essentially it estimates how much the predicted pattern must be shifted in space to cover all of the observed values.

Consider the segment of area $A(x_o, \theta)$ sketched in Fig. 1 which is defined by its position on polar coordinates, (r_i, θ_i), centered on the emission point and an angular displacement, $\delta\theta$. The area is bounded as shown by $\theta_i+\delta\theta$, $\theta_i-\delta\theta$, $r_i(1+\delta\theta)$, and $r_i(1-\delta\theta)$. The calculated concentration field within the area A is bounded by lower and upper values which we define as $C_c^l(A)$ and $C_c^u(A)$, respectively. Given observed concentrations $C_o(x_i)$ at a number of

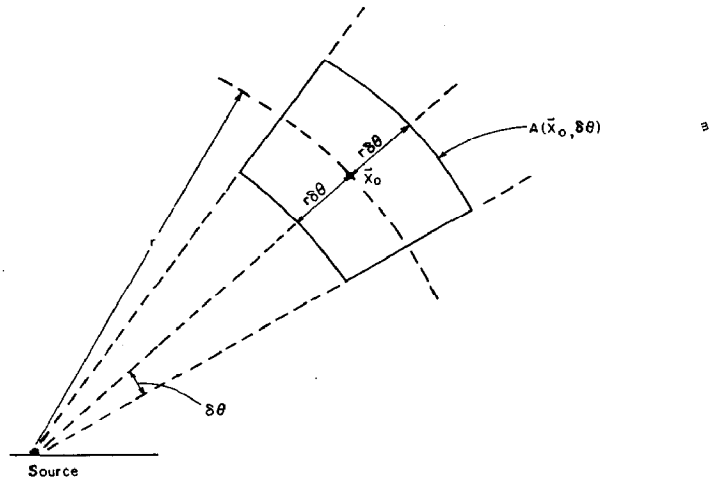

Fig. 1. Schematic of the area segment, $A(x_i, \delta\theta)$.

points $i=1, 2, 3,...M$, one can assign calculated concentrations at these points as a function of $A(x_i, \sigma\theta)$:

$$\begin{aligned} C_c(x_i, k_i) &= C_c^l(A) \text{ if } C_o(x_i) < C_c^l(A) \\ &C_o(x_i) \text{ if } C_c^l(A) < C_o(x_i) < C_c^u(A) \\ &C_c^u(A) \text{ if } C_o(x_i) > C_c^u(A) \end{aligned} \tag{1}$$

One now calculates the fraction of the test points, f_N, which yield calculated concentrations within a specified ratio N of the observed values within the sector areas defined by $\delta\theta$.

$$f_N(\delta\theta, N) = \frac{1}{M}\sum_{i=1}^{M} H\left\{N - \exp\left[\left|\ln\left(\frac{C_c(x_i, \delta\theta)}{C_o(x_i)}\right)\right|\right]\right\} \tag{2}$$

with $H\{f\}$ the Heavyside step function equal to 1 or 0, depending upon whether $f \geq 0$ or $f < 0$, respectively.

A plot of $f_N(\delta\theta, N)$ gives a direct measure of how the laboratory predicted spatial distribution compares with the observations. As an example, consider Fig. 2, from a comparison of the mass consistent MATHEW/ADPIC numerical model with some field data. For $N=2$, the figure shows that 90% of the observations are covered by a shift of 15° in the pattern, and that this rises to 100% for a 25° shift. Most emergency planners should be happy to expand a potentially affected area by only 15° to cover model uncertainty.

Ideally the sum of eqn. (2) should include all points where either the calculated or the observed concentrations are greater than background; however, it can only be applied at points where observed values are available. Lewellen and Sykes note it is possible to create artificial patterns of high and low con-

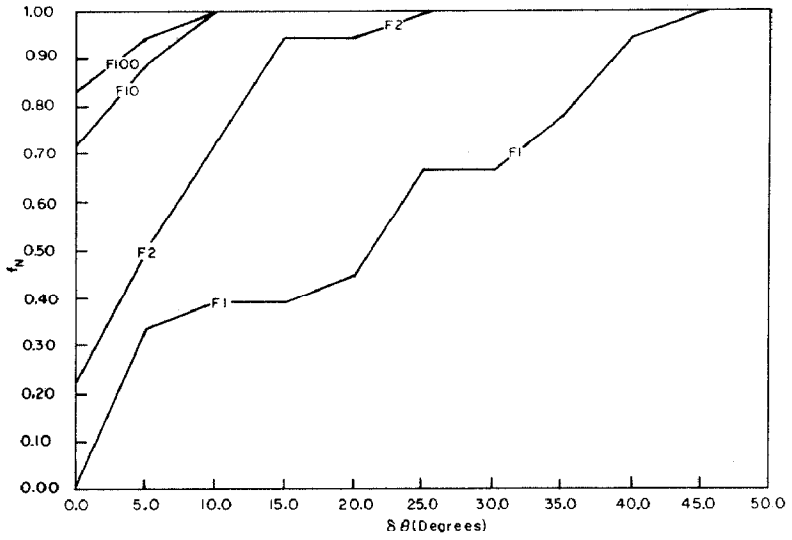

Fig. 2. Pattern test result using the MATHEW/ADPIC numerical model against a typical set of field data. f_N equals the fraction of data points covered within a factor of N by the calculated pattern expanded through an angle $\delta\theta$ [1].

centrations which would yield high values of f_N; however, such patterns would not be created by any physically consistent modeling technique.

3.0. Specific laboratory/field comparison studies

Puttock, Blackmore and Colenbrander [2] identified over 22 field experiment programs on dense gas emissions. A number of these experiments have been simulated in fluid modeling facilities. This section will examine the evidence for model similarity between some of the more recent model/field comparison studies. Table 1 summarizes prototype, model, and similarity parameter characteristics for each test series. All patterns comparison figures are grouped together in Appendix A. Section 3.8 summarizes total model/field comparison performance.

3.1 AGA Capistrano tests

Field measurement program

The American Gas Association sponsored a series of more than 30 LNG releases into diked land areas from 1.8 m to 24.4 m in diameter in 1973 near San Clemente, California [3]. One of these tests (AGA Test No. 44) was subsequently modeled by Meroney et al. [4]. LNG was pumped into a 24.4 m diameter land area surrounded by an insulated wall dike 0.5 m high. The test

area was essentially flat, with vegetation and minor roughness removed by grading an area about 100 m wide and 300 m long. Thirty six catalytic combustion sensors (MSA) were distributed over the test area on short towers. Twenty one sensors were mounted about 15 cm above the ground on five arcs ranging from 24 m to 293 m downwind. The MSA sensors are double-valued above about 10% concentration methane; hence, they are really reliable only below 7% concentration, to an accuracy of about $\pm 10\%$ of the reading.

There appears to be a large uncertainty in source volume and boil-off rate. Some investigators presumed a constant boil-off to about 80 seconds, followed by an exponential fall, others projected an exponential decaying source strength from zero time. Model experiments were performed to examine both scenarios. AGA Test 44 conditions are summarized in Table 1.

Model measurement program

The spill site was simulated at a 1:106 scale using a circular-source plenum with a porous punched plate upper surface, which emitted carbon dioxide at room temperature. Concentrations were measured with an aspirated hot-film anemometer system, accurate for carbon dioxide to about $\pm 10\%$ of reading. Variable boil-off rates were produced by using a programmed cam to modulate a micrometer needle valve in the source supply line, to follow characteristic prototype vapor release rates calculated from liquid-level measurements. Two vapor release scenarios were studied: Case I, with a constant boil-off to about 80 seconds, followed by an exponential fall, and Case II, with an exponentially falling vapor production rate from an initial maximum. These two cases bracket the maximum values used by Havens and Spicer [5] in their comparison of this case against the DEGADIS model. Case II boil-off is now considered more likely to be correct. Measurements were made on and off plume centerline for equivalent distances of 48 m to 293 m from source center. Data taken from Meroney et al. [4] have been corrected for source strength effects as suggested in Meroney [6].

Model/field comparisons

Capistrano Model Case I yielded consistently higher concentrations than that of the Case II test, which is to be expected because it describes a higher boil-off rate. Peak concentrations measured for both cases are larger than peak values detected by the MSA sensors; however it is likely that the field sensors were limited by response time. The model did not predict the large and intermittent concentration peaks at late times that were observed in the field. These peaks may be due to gustiness and changes in wind direction and speed that are present in the atmosphere, but are not present in the wind tunnel.

Figure A-1 presents the results of the pattern test analysis for the Capistrano 44 test and Case II model measurements. For $N=1$, a spatial shift of only 10° would provide 100% agreement between model and test results. Considering

TABLE 1a

Prototype and model conditions

		Continuous releases: Prototype									
Test configuration	No. Field	Specific gravity	Q (m^3/s)	D (m)	u (m/s)	u^* (m/s)	u^* (m/s)	Z_o (cm)	P.G. Stab.	$(C_{po}/C_{pa})^*$	Humidity (%)
AGA Capistrano [4]	44	1.55	40.0*	24.4	5.4	0.22		1*	C*	1.22	45
China Lake (Avocet)	18	1.55	14.9	20.0*	6.7	0.28		0.02	C	1.22	16
5 m^3 LNG [8]	19	1.55	20.1	20.0*	5.1	0.21		0.02	C–D	1.22	29
	20	1.55	13.3	20.0*	12.4	0.51		0.02	D	1.22	15
	21	1.55	18.0	20.0*	4.9	0.20		0.02	C	1.22	21
China Lake (Burro)	4	1.55	46.0	24.6	9.6	0.40	0.30	0.02	C	1.22	2
40 m^3 LNG [11,13]	5	1.55	44.1	24.0	7.8	0.33	0.37	0.02	C	1.22	6
	7	1.55	55.8	27.0	8.8	0.37	0.29	0.02	D	1.22	7
	8	1.55	60.8	28.2	2.0	0.07	0.14	0.02	E	1.22	5
		1.55	60.8	28.2	2.0	0.07	0.14	0.02	E	1.22	5
		1.55	60.8	28.2	2.0	0.07	0.14	0.02	E	1.22	5
		1.55	60.8	28.2	2.0	0.07	0.14	0.02	E	1.22	5
		1.55	60.8	28.2	2.0	0.07	0.14	0.02	E	1.22	5
	9	1.55	69.9	30.1	6.1	0.25	0.28	0.02	D	1.22	12
		1.55	69.9	30.1	6.1	0.25	0.28	0.02	D	1.22	12
Health & Safety Executive Water spray tests [29]	46 no spray	2.35	0.4	17.0*	1.7	0.10		0.65	D*	1.28	–
	46 with spray	2.35	0.4	17.0*	1.7	0.10		0.65	D*	1.28	–
Maplin sands tests [2]	46	1.90	11.3	15.1*	8.1	0.28		0.03	D	1.14	71
		1.90	11.3	15.1*	8.1	0.28		0.03	D	1.14	71
		1.90	11.3	15.1*	8.1	0.28		0.03	D	1.14	71
	54	1.85	9.3	13.8*	3.8	0.13		0.03	D	1.14	85
		1.85	9.3	13.8*	3.8	0.13		0.03	D	1.14	85

Instantaneous releases: Prototype

Test configuration	No.	Specific gravity	V (m^3)	D (m)	u (m/s)	u^* [+] (m/s)	Z_o (cm)	P.G. Stab.		Humidity (%)
Porton Downs, U.K.	3	2.30	40.0	3.9	5.5	0.25	0.2	D	–	–
40 m^3 [14,15]	8	2.00	40.0	3.9	0.5	0.02	0.2	F-G	–	–
	21	1.30	40.0	3.9	4.7	0.21	2	B-C	–	–
	29	3.56	40.0	3.9	4.3	0.19	0.2	C	–	–
	33	2.08	40.0	3.9	2.0	0.09	1	B-C	–	–
	37	1.89	40.0	3.9	5.1	0.23	1	C-D	–	–
Thorney Island, U.K.	7	1.78	2000.0	14.0	3.2	0.13	1	E	–	81
1000 m^3 [19,21,22]	8	1.63	2000.0	14.0	2.4	0.12	0.3	D	–	88
	11	2.03	2000.0	14.0	5.1	0.26	1	D	–	77
	13	1.96	2000.0	14.0	7.5	0.38	1	D	–	74
		1.96	2000.0	14.0	7.5	0.38	1	D	–	74
		1.96	2000.0	14.0	7.5	0.38	1	D	–	74
	15	1.41	2000.0	14.0	5.4	0.27	1	C-D	–	88
		1.41	2000.0	14.0	5.4	0.27	1	C-D	–	88
		1.41	2000.0	14.0	5.4	0.27	1	C-D	–	88
	18	1.87	2000.0	14.0	7.4	0.30	1	C	–	

[+] Reanalysis of Burro velocity profiles [11].

$(Ri)_c = g(SG-1)Q/[u^3 D]$

$(Ri)_l = g(SG-1)V^{0.33}/u^2$

$(Ri^*)_c = g(SG-1)Q/[u^*(u^*)^2 D]$

$(Ri^*)_l = g(SG-1)V^{0.33}/(u^*)^2$

Volume ratio $= Q/(u D^2)$

$(Re) = u D/n$

$(Re^*) = (u^*)Z_o/n$

$Pe^*/Ri^* = (u^*)^3[g(SG-1)D]$

* Symbol identities estimated conditions when associated with table values.

P.G. = Pasquill-Gifford stability category.

TABLE 1b

Prototype and model conditions

Continuous releases: Models

Test configuration	No. Field	No. Test	Scale ratio	Specific gravity	Q (cc/s)	D (cm)	u (cm/s)	u^* (cm/s)	u^* + (cm/s)	Z_o (cm)	P.G. Stability
AGA Capistrano [4]	44	11	106	1.4	340	23.0	52	2.13		0.02	D
China Lake (Avocet)	18	18	85	1.38	186	23.5	60	2.70*		0.02	D
5 m³ LNG [8]	19	19	85	1.38	251	23.5	46	2.07*		0.02	D
	20	20	85	1.38	166	23.5	112	5.04*		0.02	D
	21	21	85	1.38	225	23.5	44	1.98*		0.02	D
China Lake (Burro)	4	4	240	1.38	44	10.2	55	4.56	4.94	0.01	D
40 m³ LNG [11,13]	5	5	240	1.38	42	10.0	45	3.76	4.29	0.01	D
	7	7	240	1.38	53	11.2	51	4.23	4.88	0.01	D
	8	8	240	1.38	58	11.7	11	0.91	1.29	0.01	D
		1	240	4.18	164	11.7	32	2.65	3.26	0.01	D
		3	85	1.38	760	33.0	18	1.22	0.81	0.01	D
		A	85	1.38	760	33.0	18	1.22	0.81	0.01	D
		B	85	4.18	2195	33.0	52	3.47	3.47	0.01	D
	9	9	240	1.38	65	12.6	34	2.82	3.27	0.01	D
		2	85	1.38	874	35.6	57	3.87	2.52	0.01	D
Health & Safety Executive Water spray tests [29]	46 no spray	–	28.9	2.35	87	59.0	32	2.18		0.01	D
	46 with spray	–	28.9	2.35	87	59.0	32	2.18		0.01	D
Maplin sands tests [2]	46	M46-1	110	1.90	89	13.7	77	3.08*		0.01*	D
		M46-21	110	4.18	167	13.7	147	5.88*		0.01*	D
		M46-22	110	1.90	72	12.6	55	2.20*		0.01*	D
	54	M54-1	120	1.85	93	13.8	38	1.52*		0.01*	D
		M54-2	120	4.18	180	13.8	75	3.00*		0.01*	D

Instantaneous releases: Models

Test configuration	No.	No. Test	Scale ratio	Specific gravity	V (cc)	D (cm)	u (cm/s)	u^* (cm/s)	Z_o (cm)	P.G. Stability
Porton Downs, U.K.	3	T3	25	2.30	2744	16.0	110	6.00	0.02	D
40 m^3 [14,15]	8	T8	25	2.00	2744	16.0	0	0.00	0.02	D
	21	T21	25	3.56	2744	16.0	86	4.50	0.02	D
	33	T33	25	2.08	2744	16.0	40	3.00	0.40	D
	37	T37	25	1.89	2744	16.0	102	6.70	0.40	D
Thorney Island, U.K.	7	T33	90	2.08	2744	16.0	40	3.00	0.40	D
1000 m^3 [19,21,22]	8	TNO8	107	4.18	1633	13.0	53	2.80	0.02	D
	11	T29	90	3.56	2744	16.0	86	4.50	0.02	D
	13	P3	90	2.00	2744	16.0	84	4.40	0.02	D
		TNO13A	107	1.96	1633	13.0	73	3.90	0.01	D
		TDO13B	107	4.18	1633	13.0	132	7.20	0.01	D
	15	P3	90	2.00	2744	16.0	84	4.40	0.02	D
		UH15A	164	1.41	450	8.5	42	2.10*	0.01	D
		UH15B	164	4.18	450	8.5	117	5.87*	0.01	D
	18	P3	90	2.00	2744	16.0	84	4.40	0.02	D

TABLE 1c

Prototype and model conditions

Continuous releases: Dimensionless parameters

Test configuration	No. Field	$(Ri)_p$	$(Ri)_m$	$(Ri)_m$	$(Ri^*)_p$ +	$(Ri^*)_m$	$(Ri^*)_m$ +	(Vol. Ratio)$_p$	(Vol. Ratio)$_m$	$(Re)_m$	$(Re^*)_m$	$(Re^*)_m$ +	Pe^*/Ri^*	Pe^*/Ri^* +
AGA Capistrano [4]	44	0.057	0.041	34.1		24.6		0.013	0.012	7973	0.28		0.16	
China Lake (Avocet)	18	0.013	0.014	7.7		6.7		0.006	0.006	9400	0.36		0.26	
5 m^3 LNG [8]	19	0.041	0.041	24.1		20.2		0.010	0.010	7207	0.28		0.12	
	20	0.002	0.002	1.1		0.9		0.003	0.003	17547	0.67		1.72	
	21	0.041	0.042	24.8		20.7		0.009	0.009	6893	0.26		0.10	
China Lake (Burro)	4	0.011	0.010	6.5	11.7	1.4	1.2	0.008	0.008	3740	0.30	0.33	1.27	1.62
40 m^3 LNG [11,13]	5	0.021	0.017	11.5	9.3	2.5	1.9	0.010	0.009	3000	0.25	0.29	0.71	1.06
	7	0.016	0.013	9.2	15.1	1.9	1.5	0.009	0.008	3808	0.28	0.33	1.01	1.56
	8	1.455	1.389	1062.8	296.9	203.0	101.0	0.038	0.039	858	0.06	0.09	0.01	0.03
		1.455	1.335	1062.8	296.9	194.7	128.7	0.038	0.037	2496	0.18	0.22	0.07	0.12
		1.455	1.473	1062.8	296.9	320.6	727.4	0.038	0.039	3960	0.08	0.05	0.02	0.01
		1.455	1.473	1062.8	296.9	320.6	727.4	0.038	0.039	3960	0.08	0.05	0.02	0.01
		1.455	1.477	1062.8	296.9	331.6	331.6	0.038	0.039	11440	0.23	0.23	0.15	0.15
	9	0.05	0.050	32.4	26.2	7.2	5.4	0.013	0.012	2856	0.19	0.22	0.30	0.47
		0.055	0.049	32.4	26.2	10.7	25.3	0.013	0.012	13528	0.26	0.17	0.78	0.21
Health & Safety Executive Water spray tests [29]	46 no spray	0.063	0.060	17.6		12.8		0.001	0.001	12587	0.22		0.05	
	46 with spray	0.063	0.060	17.6		12.8		0.001	0.001	12587	0.22		0.05	
Maplin sands test [2]	46	0.012	0.013	10.4		7.9		0.006	0.006	7033	0.10		0.22	
		0.012	0.012	10.4		7.5		0.006	0.006	13426	0.20		0.72	
		0.012	0.030	10.4		19.0		0.006	0.008	4620	0.07		0.08	
	54	0.102	0.102	87.6		64.0		0.013	0.013	3496	0.05		0.03	
		0.102	0.097	87.6		60.3		0.013	0.013	6900	0.10		0.10	

Instantaneous releases: Dimensionless parameters

Test configuration	No.	$(Ri)_p$	$(Ri)_m$	$(Ri^*)_p$	$(Ri^*)_m$			$(Re)_m$	$(Re^*)_m$	Pe^*/Ri^*
Port Downs, U.K.	3	1.441	1.473	697.4	494.9	–	–	11733	0.80	1.88
40 m^3 [14,15]	8	134.116	–	83822.5	–	–	–	0	0.00	0.00
	21	0.455	0.465	228.1	44.6	–	–	10027	9.60	33.38
	29	4.642	4.744	2377.7	1732.7	–	–	9173	0.60	0.40
	33	9.053	9.252	4470.5	1644.7	–	–	4267	8.00	0.28
	37	1.147	1.172	564.1	271.7	–	–	10880	17.87	3.83
Thorney Island, U.K.	7	9.397	9.252	5693.6	1644.7	–	–	4267	8.00	0.28
1000 m^3 [19,21,22]	8	13.493	13.054	5221.5	4677.0	–	–	4593	0.37	0.08
	11	4.885	4.744	1879.6	1732.7	–	–	9173	0.60	0.40
	13	2.105	1.942	820.1	708.0	–	–	8960	0.59	0.96
		2.105	2.077	820.1	727.8	–	–	6327	0.16	0.70
		2.105	2.104	820.1	707.3	–	–	11440	0.29	1.33
	15	1.734	1.942	693.8	708.0	–	–	8960	0.59	0.96
		1.734	1.745	693.8	697.9	–	–	2380	0.08	0.26
		1.734	1.744	693.8	692.8	–	–	6630	0.23	0.72
	18	1.960	1.942	1192.5	708.0	–	–	8960	0.59	0.96

the field test measurement errors and the large uncertainty in source strength, this must be considered a quite acceptable prediction.

3.2 DOE 5 m^3 LNG China Lake spills (Avocet Series)

Field measurement program

During a 3-month period in the early fall of 1978 a series of four liquefied natural gas experiments were performed at the Naval Weapons Center (NWC) at China Lake, California [7]. Each of the four experiments variously referred to as LNG Tests No. 18, 19, 20, and 21 (or Avocet 1, 2, 3, and 4) involved the release of about 5 m^3 of LNG through a 20 cm diameter pipe onto a pond of water at a rate of about 5 m^3/min. Field concentration measurements were made over two independent measurement grids. The NWC established a grid of ten MSA catalytic combustor sensors on a square grid, and the Lawrence Livermore National Laboratory (LLNL) provided eight towers distributed in a V-shaped array with a variety of concentration sensors, thermocouples, and grab samplers. Subsequent analysis suggested that the MSA sensors did not respond to the methane cloud, either because the peak concentration fluctuations were too rapid for the catalytic sensor, or the concentrations were above the sensor limit of 7%.

Model measurement program

A 1:85 scale model of the China Lake topography was examined in a meteorological wind tunnel by Neff and Meroney [8]. Argon was released from a circular plenum centered in the middle of the test site pond. The model source gas was released from a 20 m equivalent diameter source area, over a step-function period of time at a constant boil-off rate. Concentrations were measured isokineticly, with an aspirated hot-film anemometer, which had an effective circular sampling area of $\simeq 1.6$ m^2 and an accuracy of about $\pm 15\%$ in the range of 5–15% equivalent methane concentrations. A summary of the prototype and model test conditions for this spill series is presented in Table 1. Test conditions were specified on the basis of tower measurements provided by NWC at a 2 m height on an upwind tower. (Later post-test evaluations showed that measurements of wind speed and direction made by LLNL from anemometers downwind of the spill site often varied markedly in magnitude and direction from the NWC values.)

Model/field comparisons

For such small spills the wind speeds were too large (4.9–12.4 m/s) to see strong density dominance. In addition, in every test there were large wind speed and wind direction fluctuations over the test periods (typically $\sigma_u \simeq 1$m/s, and $\sigma_\theta \simeq 10°$). In all field tests but the LNG-21 case, only the edge of the field plume touched the LLNL test grid. Although the background atmosphere was

fairly dry (16 to 29% relative humidity), Haselman [9] compared plume temperatures and concentrations to the predictions of adiabatic mixing theory, and he concluded that condensed water initially evaporated from the pond may have increased plume temperatures during spills LNG 18, 19 and 21.

For LNG-18, 19, and 20, it is likely that the mean wind directions provided by NWC were in error; hence, the model plumes do not overlay the field data. For these tests the decay of the concentrations with distance from the source appears to agree, but the direction of the plume is different. The most measurement locations were examined for the LNG-20 and 21 models (47 and 91 points respectively). Fortunately, during the LNG-21 test, the LLNL test grid and the model test grid fully overlapped.

Figures A-2–A-5 present the results of the pattern test analysis. The poor showing for LNG-18, 19, and 20 are most likely due to the misalignment of the model due to incorrect wind orientation information. The wind speed variations noted could also explain $\pm 50\%$ variation in concentration magnitudes. The patterns for LNG-21 are quite good; for $N=1$ a spatial shift of only 12.5° would provide 100% agreement between model and test results.

3.3 DOE 40 m^3 LNG China Lake spills (Burro series)

Field measurement program

The Burro series of nine LNG spill experiments were performed at the Naval Weapons Center, China Lake, California during late summer 1980 over a pond area which had been resculptured with earth moving equipment to reduce slopes along the pond banks [10]. The LNG volumes released on water ranged from 24 to 39 m^3, at rates from 11.6 to 18.4 m^3/min. Ninety gas sensors were distributed over an array of 30 measurement sites arranged in four arcs from 57 m to 800 m downwind from the center of the spill pond. Twenty wind-field stations were located at regular intervals from 800 m upwind to 900 m downwind, and 5 turbulence stations were located along the concentration sensor arcs. Thirty three of the sensors were fast response (3–5 Hz) infra-red detectors capable of measuring even in dense fogs to within $\pm 1\%$ methane, and forty five were solid-state sensors which turned out to be less reliable producing uncertainties of ± 20–30% below LFL and up to $\pm 50\%$ errors at higher concentrations. The remaining sensors were MSA catalytic devices, reliable only below 10% concentrations to about 10% of reading. The reported concentrations are based on a 10 s averaging time; the lowest sensor position was 1 m above ground. Table 1 summarizes the relevant field conditions for Burro Tests 4, 5, 7, 8, and 9. The turbulent processes in the lower atmospheric boundary layer appeared to dominate the transport and dispersion of gas for all experiments except Burro 8. Burro 8 was conducted under very low wind-speed conditions; hence, only during this test were density effects dominant. Energetic

rapid phase transition (RPT) explosions which occurred during the Burro 6 and 9 tests influenced the plume dispersion, and damaged the facility.

Model measurement program

Five different field tests, Burros 4, 5, 7, 8, and 9 were simulated in a meteorological wind tunnel [11–13]. Burro 8 was simulated over two model scales (1:240 and 1:85) and with two different simulant gas specific gravities (1.38 and 4.18). Burro 9 was simulated over the two model scales but only with the 1.38 simulant gas specific gravity. Burro 4, 5, and 7 were similated over one model scale (1:240) and with one simulant gas (1.38). Model conditions are summarized in Table 1. Since there was no data on the variable area and variable volume nature of the different LNG tests, the source conditions were approximated by providing a steady source rate for the duration of the spill over a constant area. Concentration measurements were made in sets of eight with aspirated hot-wire anemometer probes. These probes were found to aspirate isokinetically over effective areas of 2.9 m^2 and 0.36 m^2 for the 1:240 and 1:85 scaled models respectively. Cumulative errors due to the combined effect of calibration uncertainties and nonlinear voltage drifting during the test time are estimated to be approximately $\pm 20\%$ of the concentration value for the range of 5–15% equivalent methane concentrations. Model tests provided an unique opportunity to examine plume variability; all tests were replicated between two to five times at each measurement location.

All model velocities were set to the average upwind speed measured at a 2 m height. Wind shear profiles for the 1:240 scale model and source gas specific gravities of 1.38 were not in very good agreement with field results. The model winds were significantly lower near the ground than in the field. However, distorted density scaling for Burro 8 ($SG=4.18$) over the 1:240 model did reproduce field wind shear. Wind speeds measured over the 1:85 scale model reproduced field results for Burro 8 and 9 very closely. Model longitudinal turbulence measurements appeared somewhat high for the Burro 8 case, but model measurements for Burro 9 were found to be very close to the field data.

Model/field comparisons

The model was oriented in the wind tunnel based on the average wind direction which occurred during the field tests. Drift in wind approach vector was sometimes substantial during the field tests. Burro 4 had significant wind direction changes, and Burro 8 experienced a steadily declining wind speed throughout the test. Unfortunately for the case of the model Runs 1, 3, and 8, which were intended to model Burro 8 the topographic model was incorrectly turned to 215° from North, rather than the 235° as specified by the field measured mean wind direction. Nonetheless, comparisons were made with the field data by rotating the measured model data 20° to coincide with the field wind direction. It is unfortunate that this mistake occurred, because Burro 8 was

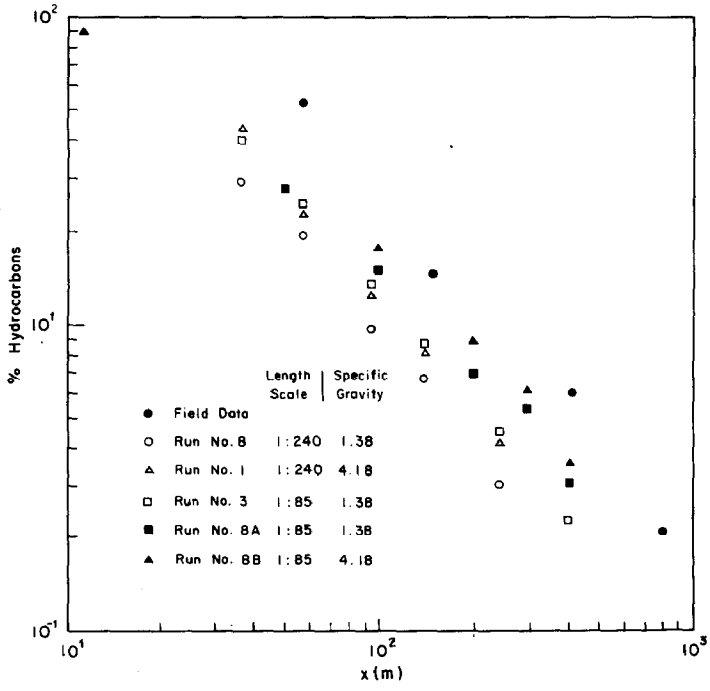

Fig. 3. Peak plume centerline concentration decay with downwind distance at 1 m height for Burro 8 [11].

the run most susceptible to the influences of topography. The comparisons of field and model data for Burro 8 and model Runs 1, 3, and 8 should therefore be viewed somewhat skeptically when drawing conclusions about model–field comparisons. Indeed it may be better to interpret Runs 1, 3, and 8 as releases performed under equivalent source and wind conditions to Burro 8, but with a different terrain orientation.

During 1984–85, model tests were performed over a new 1:85 scale model of the China Lake terrain for the Burro 8 flow conditions. These new tests (Model Runs 8a and 8b) were correctly oriented to the wind, used improved instrumentation, and used argon and freon as simulant gases, respectively. As shown in Figs. 3–5 the model experiment reproduced the unique bifurcated lobed pattern seen during the field experiment. Maximum downwind concentrations for Run 8b agree very well with field measurements; although the model case did not reproduce the elevated plume behavior seen in the non-isothermal field plume.

Field–model comparisons for each of the five different Burro tests simulated are summarized below:

- The 1:240 scale model of Burro 4 reproduced the peak centerline concentration decay with downwind distance. The arrival and departure concentra-

Fig. 4. Ground-level concentration extent comparison between Burro 8 and Run 8a, scale 1:85, $SG_m = 1.38$ [13].

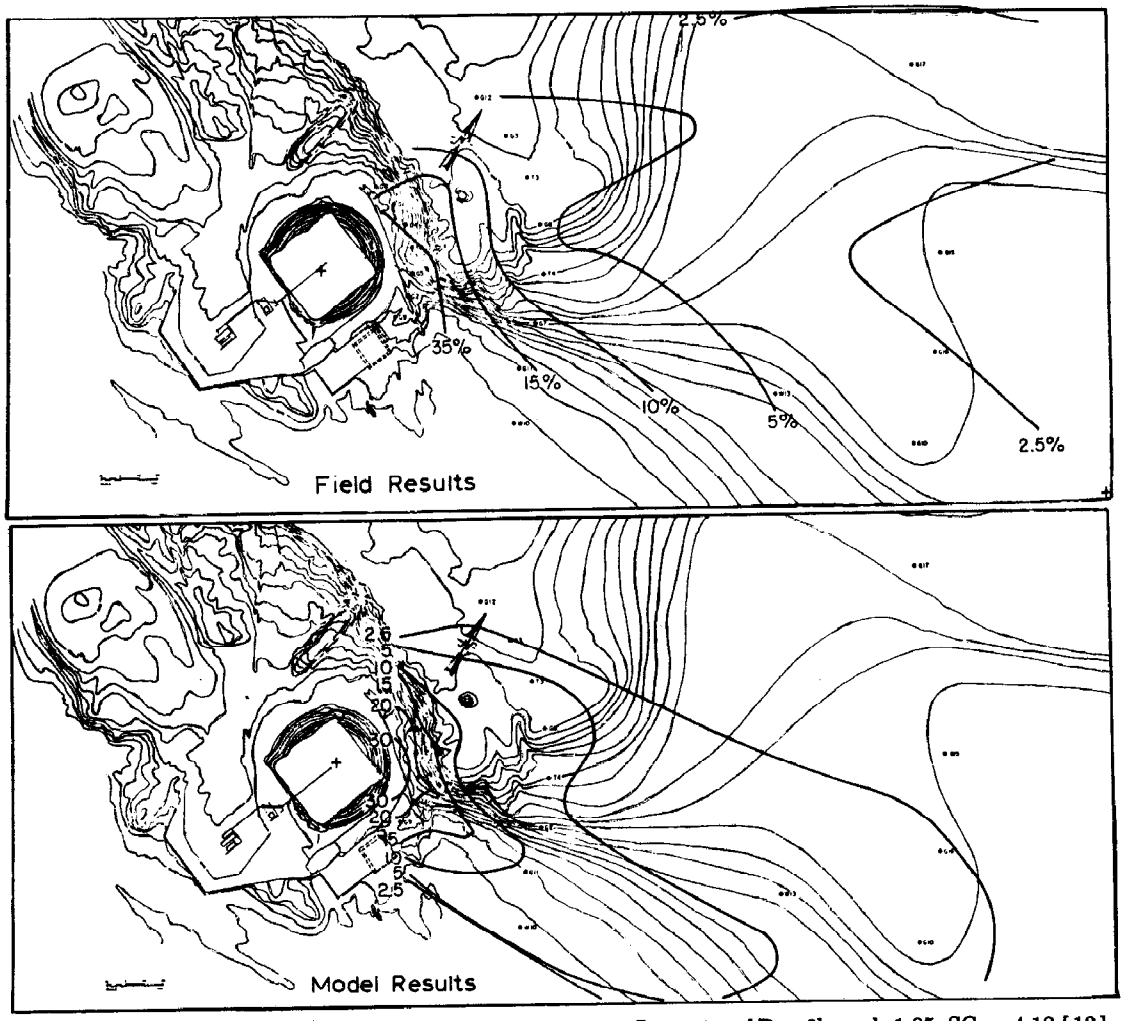

Fig. 5. Ground-level concentration extent comparison between Burro 8 and Run 8b, scale 1:85, $SG_m = 4.18$ [13].

tion structure of the model plume was significantly different from the field because of poor modeling of the approaching wind profile at a 1:240 scale. Lateral plume extent comparisons indicate that deviations in the mean wind direction in the field caused the field plume to be wider than the model plume.

- The 1:240 scale model of Burro 5 displayed all the same comparison characteristics as that of Burro 4 above. In addition, the concentrations in the interior of the field plume fluctuated much more than in the model plume. This difference is attributed to the highly turbulent atmosphere as a result of an unstable potential temperature gradient into which the plume was released. The model simulation was performed in a neutral wind field.
- The 1:240 scale model of Burro 7 did not reproduce the centerline concentration decay with downwind distance. This disagreement is attributed to the Burro 7 plume being very narrow. It is likely the plume center missed the field concentration sensors. The model plume arrived later and persisted longer than the field plume. Model wind speeds below the reference height were less than the scaled field values. Lateral plume extent comparisons indicate that deviations in the mean wind direction observed in the field caused the field plume to be wider than the model plume. This wind direction variation often caused the plume to leave the bounds of the field sensor array.
- Five different model simulations were considered for Burro 8. Three of these (Model Runs 1, 3, and 8) were performed with a 20° topographical model orientation error. Distortion of the plume initial density to obtain higher wind tunnel operating speeds resulted in significant improvement in approach wind characteristics and the avoidance of molecular diffusion effects; however, the distorted density did produce significantly different concentration histories. The 1:85 scale model with an isothermal Freon simulant (Run 8b) reproduced maximum concentration decay rates, lateral plume dimensions, and plume bifurcation. Field plume thermal effects definitely caused some plume lofting in Burro 8; this effect was not simulated by the isothermal physical model.
- Two different types of model simulations were made for the Burro 9 plume. One was at the standard scale of 1:240, and the other was at a scale of 1:85 to better approximate the mean shear and total turbulent intensity reported in the Burro 9 wind field summary. Both simulations show good agreement with field data for the peak centerline concentration decay with downwind distance. The arrival and departure time structure of the model concentration time histories was greatly improved for the 1:85 scale model. Overall, the 1:85 scale model simulation of Burro 9 had excellent agreement with field data.

Pattern comparison plots for the Burro Series model–field comparisons are provided as Figs. A-6–A-12. Pattern comparisons were not performed for Runs 1, 3, and 8 because of the orientation error. The patterns show improved model–field agreement as one changes from the 1:240 to 1:85 model, and from

an argon to a freon simulant. A pattern angle shift from 15° to 20° produces 100% agreement with field data for $N=1$. A shift from 10° to 15° produces agreement within a factor of $N=2$ for all tests.

3.4 HSE Porton Downs experiments

Field measurement program

The field trials used a gas source in the form of a cubical box of about 3.5 m side containing 40 m^3 of gas [14]. The gas was released by allowing the sides of the box (made of thin pleated tarpaulin material) to collapse to the ground under gravitational forces in about 0.8 s, essentially leaving a cube of dense gas suddenly exposed to the wind. The top surface of the box remained fixed in place during the experiment. A total of forty two individual trials were run, covering a range of wind speeds (<0.5–7.2 m/s), released gas density (specific gravity from 1.03 to 3.4), surface roughness ($z_o=2$–150 mm), atmospheric stability (Pasquill stability glass from B to F) and ground slope ($\beta=0°$–4.4°). Movement of the gas cloud was recorded by marking it with orange smoke and filming it, usually from the side and overhead. Measurements of the gas concentration were made with total integrated dosage monitors (bag samplers or absorptive charcoal) and continuously reading concentration monitors (Lovelock workfunction detectors; maximum of ten in one test). Hall et al. [15] reflect on the possibility that the dosage monitors were in error, since they typically provided integrated concentrations up to an order of magnitude smaller than the continuous monitors. Hall et al. also suggest that the time response of the continuous monitors may be between 0.5–5 s, as opposed to the 50 ms quoted by Picknett [14].

Model measurement program

Six of the trials were picked for reproduction at a model scale of 1:25 by Hall et al. [15]. Table 1 summarizes the characteristics of the field and model tests selected. Trial 3 was carried out on a 1 in 13 upward slope and yet was at similar conditions to Trial 37. Trial 8 was carried out in a very light wind, so for modeling purposes it was considered to have been carried out in still air. Hall et al. adjusted tent densities to account for the partial filling apparent in the field cinema films.

A model of the atmospheric boundary layer about 1 m deep was generated using a Counihan type system followed by a fetch of rough surface. A model of the Porton collapsing tent source was constructed at a scale of 1:25 from square bellows material, which could collapse completely into a close fitting slot in the ground. The walls collapsed in a model time of 0.18–0.25 seconds which compares well with a scaled model collapse time of 0.17 s. Model simulant was the refrigerant BCF mixed with air. The gas concentration detector was an aspirated hot wire system into which air was drawn. Lower resolution was

about 0.02% of BCF, accuracy was about ±10% of reading, and the upper frequency limit of the detector was about 20 Hz. Each experiment was replicated three times. Smoke tagged gas clouds were photographed to compare with field pictures. Wind speed profiles were measured with a pulsed-wire anemometer.

Model/field comparisons

Hall et al. provided side-by-side comparison of photographic sequences of the Porton release series. These photographs exhibit truly remarkable model reproduction of the shape and appearance of the field releases. The wind-tunnel model reproduced the size, shape, spread rates and downwind travel distances as well as detailed reproduction of the characteristic cloud features. The model exhibits the rapid initial collapse to a low, even, height; the curved, sharply faced, upwind face including a rotating vortex; and the horseshoe-shaped downwind edge. Measurements of cloud width and downwind travel times are also generally very good. Hall et al. concluded their model clouds were the same thickness as the full scale to within the "determinable level of accuracy".

Direct comparison between model and field concentration data present a much more confusing picture. In some cases the agreement is good, but sometimes quite poor. During Run 37 the field continuous monitors and the model results are quite close, whereas during Run 33 the field measurements are significantly lower than the model values. During Runs 3 and 8, integrated doses from field bag samplers were generally of the same order as field and model continuous samplers when measurements were made at the same station. During the rest of the runs the Porton charcoal buttons produced dosimeter measurements up to an order of magnitude less than field or model continuous measurements. Post-facto analysis of the equipment showed the carbon buttons to be sensitive to temperature, humidity, gas concentration, wind speed, and even direction.

Differences also exist between the full-scale and model continuous measurements in both magnitude and variability. Realization-to-realization variations can explain up to an order of magnitude difference between the largest and smallest concentrations. Variation in arrival time of the experiments seem to fall within the amount allowed by local cusp variations in the cloud shape. As quoted from Hall et al.: "With such large possible levels of variability in the concentration/time traces from both the model and the full-scale, almost any level of agreement levels within an order of magnitude for single realisations (sic) of the experiment might be classed as good agreement"!

Two qualitative differences between the appearance of the model and full-scale concentration/time traces are apparent: (a) a sharp high initial peak in concentration appeared during the model experiments in locations near the source, and (b) much higher levels of fluctuations occurred during the model

experiments compared with the full scale. The high initial peak of the gas cloud is clearly associated with the gravity-driven head vortex. It was not detected by the field sensors; however, the location of the peak is very sensitive to field detector location and response time. The model sensor is believed to have excellent spatial and time resolution (20 Hz model scale, or about 4 Hz full scale), whereas aerodynamic characteristics of the field sensor alone suggest a full-scale frequency response of 1 Hz, and apparent smoothing of the concentration data suggests an actual response of 0.2 Hz [15].

The density of field and model data reported did not justify plotting pattern comparability.

Both the Porton Downs and the following Thorney Island experiments considered situations where an initially quiescent cloud collapses to the ground. The collapse itself produces enough kinetic energy and turbulence to dominate the mixing process. Hence, parameters such as approach wind speed, thermal stratification, and surface roughness are unlikely to make significant changes in the dense cloud dilution rate over the distances monitored. Spills of LNG or LPG which result in generation of a vapor cloud over a finite period of time produce clouds which have small depth/width rations; thus, they do not produce strong collapse-related turbulence.

3.5 NMI Thorney Islands experiments

Field measurement program

Between 1982 and 1984 a series of 29 experiments were performed at an airfield at Thorney Island, West Sussex, U.K., in which 2000 m^3 of gas of various densities were released in both unobstructed and obstructed configurations [16]. The data obtained were very comprehensive, including concentration, turbulence, visual records, and detailed meteorological information. Up to 100 gas sensor records were obtained in individual trials at distances up to 750 m from the release point. The fully developed field of 45 measurement stations carried a total of 215 transducers, 183 being gas sensing devices and 32 environmental sensors. The standard gas sensors used an oxygen depletion concept to cause variations in an electrochemical cell. These sensors had a frequency response of 1 Hz [17].

The field release volume was a twelve-sided polygon tent which was about 14 m diameter and 13 m high containing a total volume of 2000 m^3. During a release a flexible top cover was withdrawn by raising it into a bundle above the gas tent cylinder. During some tests permeable or impermeable vapor barriers of various heights were placed downwind of the dense gas releases. Only part of the Thorney Island data has been made available to the scientific community at this time [18]; hence, only a few physical model comparison experiments have appeared.

Model measurement program

Three organizations have reported model simulation experiments of six of the Thorney Island trials [19–22]. The details of the trials selected and the model scales used are recorded in Table 1. Scale ratios used varied from 1:90 to 1:164. The collapsing tent source was simulated by a cubical volume with a collapsing bellows [19], or by a plastic truncated cylinder which was retracted downward by gravity beneath the tunnel floor at the time of release. All laboratory investigators used aspirated hot wire anemometer systems to detect continuous gas concentrations. Model experiments were replicated from 3 to 5 times each.

Hall and Waters [19] compared three of the tests performed by Hall et al. [15] to Thorney Island trials 7, 11, 13, 15 and 18. The field tests selected for comparison were chosen because they had dimensionless bulk Richardson number parameters close to the model values examined by Hall et al. (i.e. field to model variations of about 10%). Trials 13, 15 and 18 were at sufficiently close Richardson number conditions to be considered repeat runs of the same operating conditions. Since from earlier tests the Richardson number seemed to be the major dominant parameter during the Thorney Island trials, deviations in field/model surface roughness, slight deviations in release configuration, and the lower source aspect ratio during the model tests were considered insignificant.

Van Heugten and Duijm [20] and Duijm et al. [21] simulated Thorney Island trials 8 and 13. Unfortunately, the intake velocity of the aspirated probes they used was about 2.8 m/s. During post-analysis of their data Duijm noted that when a probe is mounted at 4 mm above a wind-tunnel floor, where the wind velocity is less than 0.8 m/s, the probe will smooth out the strong concentration gradients near the surface, and the concentration recorded would be systematically less than the actual concentration at probe position.

Schatzmann et al. [22] reported results from model simulations of Thorney Island trial 15 in their open circuit meteorological wind tunnel. Details of their experiment were not described, but they did perform measurements with both equal and distorted specific gravity, while maintaining constant Richardson number.

Model/field comparisons

Given that in the Hall and Water [19] comparisons the model was not an exact representation of the trial either in source form or operating conditions, the general level of agreement was remarkably good. Dominance of the cloud dilution by turbulence produced during initial collapse may explain the tolerance of the comparison. Photographic comparisons between field and model displayed similar size, spread and travel rates. Concentration measurements are also comparable, but not in all cases identical. Overall, nearly all the peak concentrations in the model are within a factor of two of the field trials.

There is one comparison between model and full scale results where consistent differences occur. In Trial 7, the model concentrations within the cloud are persistently lower and the model cloud persists over the samplers considerably longer than the field case. Hall and Waters attribute this difference to the larger surface roughness in the model experiment, low plume Reynolds numbers, and deep boundary sublayers. The effect is very similar to that seen during modeling experiments performed by Neff and Meroney [23] for the Burro series when a model scale of 1:240 produced high model shear rates and lower near surface wind speeds than during full scale conditions.

Schatzmann et al. [22] provided time duration plots for only two locations during their model tests of Thorney Island trial 15. The time of arrival, departure, peak concentrations, and fluctuations are all similar for undistorted density scaling. The peak concentrations are similar during the distorted density scaling situation, but the arrival and departure times are distorted.

3.6 Shell Maplin Sands experiments

Field measurement program

In 1980 Shell Research, Ltd. performed a series of controlled spills of LNG and refrigerated propane in quantities up to 20 m^3 on the sea at Maplin Sands in the South of England [24]. Release of the liquid was either continuous or instantaneous. Continuous spills released liquid at a steady rate from the end of a pipe at or near the water surface. For instantaneous spills the liquid was poured into an open-topped insulated octagonal barge, 12.5 m across, which was then submerged, created the spill as water flowed in to displace the liquefied gas. Model studies of only two of the continuous spills of propane (Runs 46 and 54) have been described by Puttock and Colenbrander [25]. These cases used an open pipe release at water level for the source. Spill 54 was performed at a moderate wind speed (3.8 m/s) for the Maplin Sands site, and displayed strong lateral and upwind buoyancy dominated spreading; whereas spill 46 was released when the wind was 8.1 m/s, and was only marginally affected by the density of the gas.

Instruments were placed on 71 floating pontoons equipped with 4 m masts. There were about 360 instruments in the array. The gas sensor used was a device based on measurement of the heat loss from a filament under free convection. The sensor had a time constant of 3 seconds, and all data was smoothed by a three-second moving average to eliminate high frequency noise spikes. A fast response thermocouple was also placed close to the lowest gas sensor, and the spills were photographed from two land-based towers and a helicopter high overhead.

Model measurement program

Shell Laboratories in Amsterdam simulated spills 46 and 54 in their wind tunnel. These tests were selected because it was expected that heat transfer

TABLE 2

Pe/Ri influence on simulation of Maplin sands LPG spills: Runs No. 46 and 54 (Shell Research, Amsterdam, The Netherlands, November 30, 1984)

Trial No.	Gas type	Scale	Specific gravity	Velocity (m/s)	LFL (m)	*Pe/Ri*
Actual						
Maplin-46	LPG	1:1	1.9	8.1	210-280	–
Wind tunnel						
MS46-1	Fr-Ar	1:110	1.9	0.77	230-290	2910
MS46-21	Fr	1:110	4.2	1.47	250-280	12120
MS46-22	Fr-Ar	1:120	1.9	0.55	140-190	1340
Actual						
Maplin-54	LPG	1:1	1.85	3.8	380-520	–
Wind tunnel						
MS54-1	Fr-Ar	1:100	1.85	0.38	250-290	357
MS54-2	Fr	1:100	4.2	0.75	450-520	1560

$Pe/Ri = U^3/(g'D)$

and latent heat release from condensed water vapor would have minimal effect during the field dispersion situations. The experiments were designed to emphasize the effect of molecular diffusion versus turbulent entrainment in the model mode. Specific concentration data was not available, but distances to LFL were reported. Projected model and field conditions are summarized in Table 1.

Model/field comparisons

Researchers at Shell Laboratory, Amsterdam, have concluded that molecular diffusion may play an important role in the laboratory when scaled turbulent diffusivity is very small [25,26]. They compared wind tunnel simulations of several of the Maplin Sands experiments to field data, as well as considering several experiments from the Neff and Meroney [23] wind tunnel series. They discovered that when the parameter ratio of Peclet number to Richardson number is less than a critical value simulations were inaccurate. Their parameter was based on the characteristic velocity and source scales, which gave:

$$Pe/Ri = U_R^3/(g'_o D), \tag{4-4}$$

where D is a molecular diffusivity. This parameter measures the relative rates of turbulent entrainment and molecular diffusion. When this parameter is too small the scaled concentrations will be smaller than field values. Table 2 contains the comparisons considered by Shell Research. A critical value of Pe/Ri based on approach wind speed at a 10 m reference height is about 1500. Since the local density difference decreases as the cloud disperses one expects molecular diffusion effects to decrease with time as the cloud moves downwind. Hence,

the criteria may be overly conservative in the presence of large initial mixing caused by collapse of a tall cloud, fences, explosions, or water spray curtains.

3.7 HSE water spray curtain tests

Field measurement program

Full-scale dispersion experiments of dense gas dispersion in the presence of water curtains were performed by the Health and Safety Executive, U.K., in 1981 using cold CO_2 vapor ($-79°C$) at an estimated spill rate of 1.1 kg/s from a point source [27]. Two of these tests were selected for simulation in the wind tunnel at a scale ratio of 1:28.9. Trials HSE 41 and HSE 46 were chosen because of availability of model-size water-spray nozzles, practicality of scaling ratios, and apparent quality of the data.

The average field wind speed recorded for HSE 41 was about 3.2 m/s for the no-spray and spray intervals. Significant field concentrations were measured at large lateral distances, this was puzzling because the buoyancy length scale ratio, l_b/L, was very small, and projections from results by Britter [28] and Neff and Meroney [11] for continuous and finite time releases always produced narrow plumes under equivalent conditions. A mass balance performed over field measurement stations for HSE 41 failed to agree with the source strength provided by HSE. Further communication with HSE personnel revealed that during subsequent tests the recording anemometer was found to produce large errors. It was likely that the wind instrument used by HSE was in the wake of other test equipment during this test; thus, field and model data for this case are inconclusive.

The wind speeds at 1.25 m for HSE 46 were reported to range from 2.9 to 1.7 m/s over the test period. The wind field was variable, and wind directions varied from 293° to 340°. Shear measurements suggested that local surface roughness, z_o, was about 6.5 mm and $u_*/u_{10}=0.06$. Groundlevel and elevated measurements were made of CO_2 concentration at six stations up and downwind of the spray curtain.

Model measurement program

The HSE tests were modeled at a scale of 1:28.9 by Meroney, Neff, and Heskestad [29]. Vortex generators and a wall trip at the wind tunnel entrance produced a boundary layer about 1 m deep over the test region with a scaled $z_o=4.3$ mm and $u_*/u_{10}=0.068$. A miniature source was constructed to reproduce the radial exhaust characteristics of the source used by the HSE researchers. Sampling points were located at equivalent field locations, and an additional crosswind ground-level sampling array was placed just downwind of the HSE field sampler array. During HSE Trial 46, the model spray curtain consisted of 20 nozzles discharging at a 10.4 cm height, spaced 5.66 cm apart, and directed vertically downward. The source gas used in all runs to simulate the cold CO_2

was a mixture of 68% CO_2, 31% CCl_2Fl_2, and 1% C_2H_6. Concentrations were measured with a flame-ionization detector to values less than 0.1% with an accuracy of ±5%. Measurements were made both with and without the water-spray curtain in operation.

Model/field comparisons

Linear and logarithmic scatter diagrams of concentrations measured for no-spray and spray configurations of HSE Test 46 at equivalent points produce correlations, r, of 0.87 and 0.97 respectively. Pattern comparisons are included as Figures A-13 and A-14.

3.8 Discussion of fluid modeling versus data comparisons

The twenty six field experiments simulated include releases exemplifying a wide range of heavy gas dispersion behavior. Continuous, instantaneous, and finite time release conditions are included, as well as cases which include topography, dikes, and water-spray curtains. Comparison of the model predictions with field observation is facilitated by the classification of the tests with a Release Richardson Number [5]. Richardson numbers are defined for continuous and instantaneous releases as follows:

Continuous releases $\quad Ri_o^c = g' Q/(u_*^2 D)$

Instantaneous releases $\quad Ri_o^I = g' V_i^{1/3}/u_*^2$

and characteristic frontal velocities are:

Continuous releases $\quad V_f = \sqrt{g' H} = \sqrt{g' Q/(uD)}$

Instantaneous releases $\quad V_f = \sqrt{g' H} = \sqrt{g' V_i^{1/3}}$

Table 3 shows release Richardson numbers calculated for the twenty six cases modeled.

Britter [30] suggested that the plume downwind of a release should be passive from the source for Ri_o^c less than about 1, and significant lateral and upwind spreading would occur for Ri_o^c greater than 10 and 40 respectively. Only one of the releases has a Richardson number near 1, nine have numbers between 10 and 40, and one has a Richardson number greater than 40.

Havens and Spicer [5] propose that when Ri_o^I is greater than 1000 the flow and dilution processes which dominate down to average concentrations of about 5% are buoyancy dominated. Most of the Thorney Island tests and a few of the Porton Island tests exceed values of 1000.

Predicted and observed values of the upper flammability limit, UFL, lower flammability limit, LFL, and LFL/2 (15 / 5 / 2.5% for LNG, 10 / 2 / 1% for

TABLE 3

Richardson number classification of field experiment releases for continuous and instantaneous spill experiments

Continuous releases								
Test configuration	No.	g' (m/s/s)	Q (m^3/s)	D (m)	u (m/s)	u^* (m/s)	$(Ri)_{o/c}$	
AGA Capistrano [4]	44	5.4	40.0*	24.4*	5.4	0.22*	33.9	L
China Lake (Avocet)	18	5.4	14.9	20.0*	6.7	0.28*	7.7	
5 m^3 LNG [8]	19	5.4	20.1	20.0*	5.1	0.21*	24.1	L
	20	5.4	13.3	20.0*	12.4	0.51*	1.1	P
	21	5.4	18.0	20.0*	4.9	0.20*	24.8	L
China Lake (Burro)	4	5.4	46.0	24.6	9.6	0.40	6.5	
40 m^3 LNG [11]	5	5.4	44.1	24.0	7.8	0.33	11.5	L
	7	5.4	55.8	27.0	8.8	0.37	9.2	L
	8	5.4	60.8	28.2	2.0	0.07	1063.1	L & U
	9	5.4	69.9	30.1	6.1	0.25	32.4	L
Health & Safety Executive	46	13.3	0.4	17.0*	1.7	0.10*	17.7	L
Water spray tests [29]	no spray							
	46	13.3	0.4	17.0*	1.7	0.10*	17.7	L
	with spray							
Maplin Sands Tests [2]	46	8.8	11.3	15.1*	8.1	0.28	10.4	L
	54	8.3	9.3	13.8*	3.8	0.13	87.1	L & U
Instantaneous releases								
Test configuration	No.	g' (m/s/s)	V (m^3)	D (m)	u (m/s)	u^* (m/s)	$(Ri)_{o/c}$	
Porton Downs, U.K.	3	12.8	40.0	3.9	5.5	0.25*	691.8	
40 m^3 [15]	8	9.8	40.0	3.9	0.5	0.02*	10,000	BD
	21	2.9	40.0	3.9	4.7	0.21*	222.1	
	29	25.1	40.0	3.9	4.3	0.19*	2348.8	BD
	33	10.6	40.0	3.9	2.0	0.09*	4420.8	BD
	37	8.7	40.0	3.9	5.1	0.23*	555.6	
Thorney Island, U.K.	7	7.7	2000.0	14.0	3.2	0.13	5596.9	BD
1000 m^3 [19]	8	6.2	2000.0	14.0	2.4	0.12	5288.9	BD
	11	10.1	2000.0	14.0	5.1	0.26	1835.3	BD
	13	9.4	2000.0	14.0	7.5	0.38	799.7	
	15	4	2000.0	14.0	5.4	0.27	674.0	
	18	8.5	2000.0	14.0	7.4	0.30	1160.2	BD

L: Lateral spreading ($Ri > 101$, U: upwind ($Ri > 40$), P: passive ($Ri < 1$), BD: buoyancy dominated ($Ri > 1000$)*: approximated values.

propane, and 15 / 5 / 2.5% for the inert gas mixtures) are compared in Table 4. The observed values were determined from the reported experimental maximum concentrations on each radial arc by drawing a visual best-fit straight line on the respective log-maximum-concentration versus log-distance plot. The percentage deviation of the predicted from the observed distances for all

TABLE 4

Comparison of observed vs fluid-model predicted maximum distances to gas concentrations in the flammable limit range

Test configuration	No.	No. test	Observed			Predicted			[Pre − Obs)/Obs] (100)			Confidence interval (90%)	
			UFL	LFL	LFL/2	UFL	LFL	LFL/2	UFL	LFL	LFL/2		
AGA Capistrano [4]	44	–	100	220	300	110	270	600	10	23	100	UFL:	Mean % deviation from PRE −9.0%
													% Standard deviation = + 22.8%
China Lake (Avocet)	18	18	–	–	–	65	130	–					
5 m^3 LNG [8]	19	19	65	–	–	85	–	–	31				
	20	20	45	70	100	27	75	125	−40	7	25	LFL:	Mean % deviation from PRE +0.4%
	21	21	70	100	–	85	–	–	21				% Standard deviation = + 22.4%
China Lake (Burro)	4	4	60	180	300	65	190	325	8	6	8		
40 m^3 LNG [11,13]	5	5	70	260	550	70	200	400	0	−23	−27		
	7	7	100	250	650	90	250	550	−10	0	−15	LFL/2:	Mean % deviation from PRE +7.8%
	8	a	150	400	700	100	300	660	−33	−25	6		% Standard deviation = +32.5%
		b	150	400	700	120	350	700	−20	−13	0		
	9	9	110	280	490	90	240	450	−18	−14	−8		
		2	110	280	490	100	290	550	−9	4	12		

Porton Downs, U.K.	3	13	–	–	–	10	21	36			
40 m^3 [15]	8	18	15	–	–	13	22	27	−13		
	21	T21	–	–	–	8	28	50			
	29	T29	–	–	–	20	31	55			
	33	T33	–	–	–	14	25	36			
	37	T37	–	–	–	10	20	36			
Thorney Island, U.K.	7	T33	60	120	180	40	90	125	−33	−25	−31
1000 m^3 [18]	11	T29	–	100	160	–	130	200		30	25
	13	P3	–	100	160	50	110	180		10	13
	15	P3	80	160	250	50	110	180	−38	−31	−28
	18	P3	–	100	140	50	110	180		10	29
Maplin Sands, U.K.	46	M46-1	–	245	–	–	260	–		6	
Propane spills [25]		M46-21	–	245	–	–	265	–		8	
		M46-22	–	245	–	–	165	–		−33	
	54	M54-1	–	452	–	–	270	–		−40	
		M54-2	–	452	–	–	485	–		7	
Health & Safety Executives	46	–	–	15	25	–	22	30		47	20
Water spray tests [29]	no spray										
	46	–	–	<6	–	–	<6	–			
	with spray										

TABLE 5

Pattern comparison plot results

Configuration		Date	Run No.	Scale ratio	Specific gravity	Points compared	Intercept of θ, Degrees			
							f-1	f-2	f-5	f-10
AGA Capistrano	Field	(1974)	44	–	1.52	–				
	Model	(1977)	44	106	1.55	4	10.0	7.5	0.0	0.0
China Lake (Avocet)	Field	(1978)	18-21	–	1.5	–				
	Model	(1979)	18	85	1.38	3	20.0	5.0	0.0	0.0
			19	85	1.38	5	15.0	5.0	5.0	0.0
			20	85	1.38	4	17.5	7.5	7.5	7.5
			21	85	1.38	6	12.5	0.0	0.0	0.0
China Lake (Burro)	Field	(1980)	4-9	–	1.5	–				
	Model	(1981)	4	240	1.38	8	20.0	15.0	12.5	7.5
		(1985)	5	240	1.38	6	15.0	12.5	7.5	7.5
			7	240	1.38	12	15.0	10.0	7.5	5.0
			8	85	1.38	17	45	15	7.5	5
			8	85	4.18	17	20.0	10.0	2.5	2.5
			9	240	1.38	13	17.5	15.0	12.5	10.0
			9	85	1.38	13	15.0	12.5	10.0	10.0
MSE Spray Tests	Field	(1981)	46	–	2.35	–				
	Model	(1983)	46	No Water Sprays						
				28.9	2.35	6	20.0	10.0	0.0	0.0
			46	With Water Sprays						
				28.9	1.35	6	12.5	5.0	0.0	0.0
FEM3 Numerical Prog.										
Heat transfer										
Terrain included										
Chan & Ermak		(1983)								
		Burro	8	1	–	13	45.0	2.5	0.0	0.0
		Burro	9	1	–	13	12.5	10.0	10.0	10.0

of the experiments simulated are also shown in Table 4. These data permit the assignment of a 90% confidence interval to the predictions of distance to UFL, LFL, or LFL/2. For example, the Burro comparisons indicate a predicted maximum distance to the LFL gas concentration which would be from 25% below to about 6% above that observed.

Pattern comparison plots

Appendix A contains the individual pattern comparison plots prepared from the peak concentration contours at ground-level. Table 5 summarizes the val-

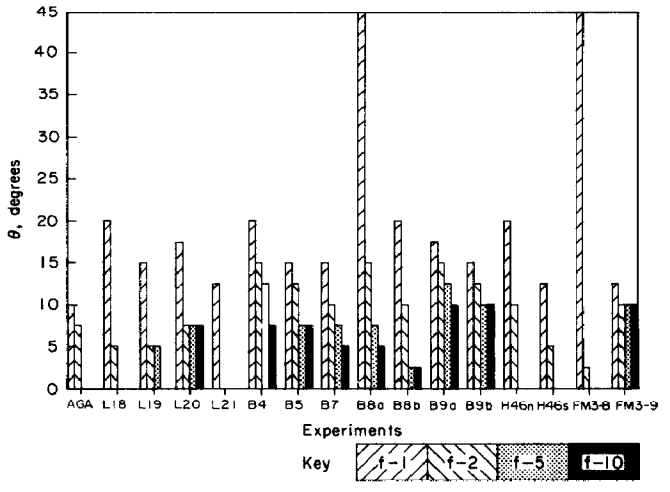

Fig. 6. Pattern comparison test summary bar chart for theta intercept (degrees).

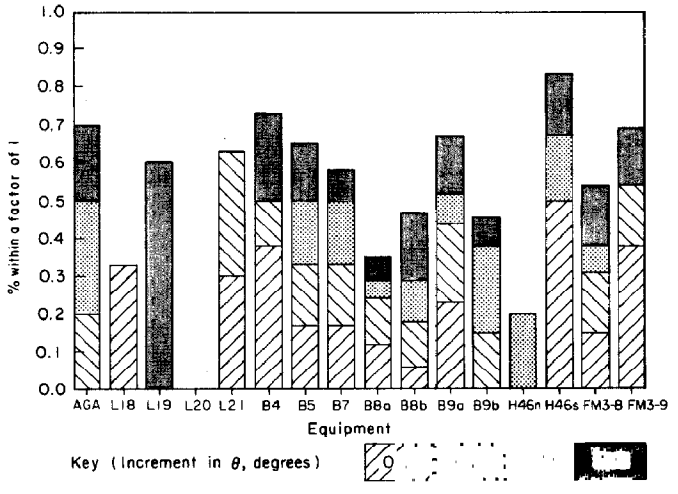

Fig. 7. Pattern comparison test summary bar chart for percent compatability at $0° \leq \theta \leq 7.5°$.

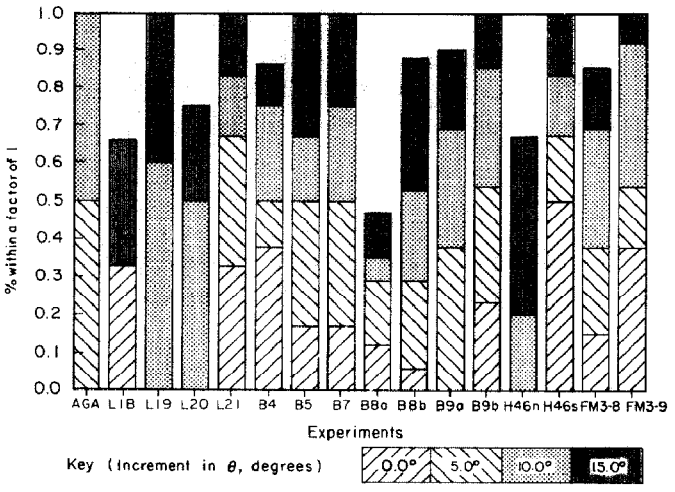

Fig. 8. Pattern comparison test summary bar chart for percent compatibility at $0° \leq \theta \leq 15°$.

ues of θ, $(\delta\theta)$ at which there exists 100% agreement between field and model data at various magnitudes of N ratio. In no case is a θ value greater than 15° required to provide agreement within a factor of 2 between field and model results. Figure 6 provides the same information in a bar chart format. Figures 7 and 8 display the percent of measured data predicted exactly for each test in terms of θ values varying from 0° to 15°.

To place these values in context with other modeling alternatives, one may consider patterns comparison plots for one of the more complicated numerical models. The FEM3 model developed at LLNL which includes terrain and heat transfer effects is among the most sophisticated primitive equation models. Chan and Ermak [31] published ground level concentration contours for Burro series tests 8 and 9. Pattern comparison plots are provided as Figures A-15 and A-16. θ shift values of 45° and 12.5° are required to produce 100% agreement with field data at $N=1$. This compares with θ values of 20° and 15° for the best comparable physical model effort. Hence, the most advanced calculations predict concentration isopleths of about the same order of spatial accuracy as physical simulation.

4.0 Summary and recommendations

Seven field experiments which included 26 separate releases of dense gas have been compared with physical model simulations in Sections 3.1 – 3.7. In Section 3.8 the ability of fluid model methods to predict UFL, LFL, and LFL/2 levels is examined. Results of the Surface Pattern Comparability Approach described in Section 2.0 are also reported in Section 3.8. The following observations are appropriate:

(a) The level of agreement obtained between model and field experiments is generally very satisfactory. The model clouds are very similar in appearance, they spread and travel at correct rates, measured concentrations compare very well, and peak concentrations are usually predicted to within a factor of two or better.

(b) Model simulations where specific gravity, volume flux ratio and Froude number equality have produced successful predictions of field concentrations are limited to situations where mean prototype wind speeds exceed 3 m/s, scale ratios do not exceed 250, and Pe_*/Ri_* ratio exceeds 0.15.

(c) During model simulations where volume flux ratio and flux Froude number equality are stipulated, peak concentration isopleths are preserved if mean prototype wind speeds exceed 2 m/s, scale ratios do not exceed 100, and Pe_*/Ri_* ratio exceeds 0.15. However, in this case the time of arrival and departure of the plumes are distorted.

(d) Field/fluid model comparisons suggest that LFL distances for LNG spills are predicted within a standard deviation of 25% with a 90% confidence level.

(e) Field/fluid model comparisons suggest that ground level concentrations are predicted exactly ($N=1$) for θ increments of less than 20°, and within a factor of two ($N=2$) for θ increments of less than 15°.

(f) The most advanced fluid modeling effort and the most sophisticated numerical models appear to predict plume concentrations within comparable levels of spatial accuracy. It may be that this is associated with an inherent limit to the prediction of single realization field experiments.

(g) It does not appear that strict specification of Richardson number, Ri_*, is necessary to obtain adequate simulation of most aspects of a field trial. However, accurate specification of friction velocity, u_*, is so difficult for both field and model measurements that it is difficult to resolve this point decisively. It does appear necessary to roughly match velocity gradient over the plume depth.

(h) Strict observance of the roughness Reynolds number criterion ($Re_*>2.5$) or the source Reynolds number criterion ($Re>3000$), does not seem to be necessary when simulating flows dominated by gas release configuration. The roughness Reynolds number may be important during simulation experiments when one is concerned with decay of concentration to levels less than 0.1%.

Acknowledgement

The author wishes to acknowledge support from the Gas Research Institute, Chicago, Illinois, USA, through Contract No. 5083-252-0962.

List of symbols

C_c	calculated or measured concentration
C_o	observed concentration
C_p	specific heat capacity
D	source diameter
Fr_a	Froude number, ambient reference density
Fr_f	flux Froude number
Fr_s	Froude number, source reference density
g	gravitational constant
Gr	Grashof number
$H(f)$	heavyside operator
k	von Karman constant
k	conductivity
l_b	buoyancy length scale
L	length scale
L_{mo}	Monin-Obukhov stability length
M	molecular weight
M	mass flux ratio
n	moles
p	power law coefficient
Pe	Peclet number
Pr	Prandtl number
Q	source flow rate
r	radius
R	gas constant
Re	Reynolds number
Re_{Da}	source Reynolds number, ambient reference
Re_{Ds}	source Reynolds number, source reference
Ri	Richardson number
Ri_b	bulk Richardson number
Ri_*	Richardson number, friction velocity
SG,sg	specific gravity
t,T	time
u,U	velocity
u,v,w	velocity components
u_*	friction velocity
V	volume flux ratio
V	gas volume
W	source gas exhaust velocity
x,y,z	Cartesian coordinates
z_o	roughness length

Greek symbols

γ	specific heat capacity ratio
δ	boundary layer depth
β	terrain slope
μ	dynamic viscosity
υ	kinematic viscosity
π	pi (3.1417)
ρ	density
σ	variance
χ	concentration

Superscript symbols

—	average
*	molar value
′	fluctuating component

Subscript symbols

a	ambient atmospheric conditions
g,o	source gas
m	model
p	prototype
R	reference

References

1 W.S. Lewellen and R.I. Sykes, A scientific critique of available models for real-time simulations of dispersion, Nuclear Regulatory Commission Report NUREG/CR-4157, 1985, 170 pp.

2 J.S. Puttock, D.R. Blackmore and G.W. Colenbrander, Field experiments on dense gas dispersion, J. Hazardous Materials, 6 (1982) 13–41.

3 AGA (American Gas Association), LNG Safety Program, Interim Report on Phase II Work, American Gas Association Project IS-3-1, Battelle Columbus Laboratories, 1974.

4 R.N. Meroney, J.E. Cermak, D.E. Neff and M. Megahed, Dispersion of vapor from LNG spills - simulation in a meteorological wind tunnel, Colorado State University, Civil Engineering Report CER76-77RNM-JEC-DEN-MM57, 1977, 152 pp. (also errata sheet).

5 J.A. Havens and T.O. Spicer, Development of an atmospheric dispersion model for heavier-than-air gas mixtures, Vol. 1, Final Report, Depot. of Transportation Contract DT-CG-23-80-C-20029, 1985, 191 pp.

6 R.N. Meroney, Guideline for fluid modeling of liquefied natural gas dispersion: Vol. II, Technical support document, Gas Research Institute Report GRI 86/0102.2, Colorado State University, Civil Engineering Report CER 84-85 RNM-50b, 1986, 263 pp.

7 R.P. Koopman, B.R. Bowman and D.L. Ermak, Data and calculations of dispersion on 5 m^3 LNG spill tests, Lawrence Livermore Laboratory Report UCRL-52876, 1979, 31 pp.

8 D.E. Neff and R.N. Meroney, Dispersion of vapor from LNG spills - simulation in a meteorological wind tunnel of spills at China Lake Naval Weapons Center, California, Final Report, Dept. of Transportation Contract No. DOT CG-75279-A, Colorado State University, Civil Engineering Dept. Rept. CER78-79DEN-RNM41, 1979, 77 pp.

9 L.C. Haselman, Effect of humidity on the energy budget of a liquefied natural gas (LNG) vapor cloud, Liquefied Gaseous Fuels Safety and Environmental Control Assessment Program: Second Status Report, Dept. of Energy, DOE/EV-0085, Vol. 2 of 3, Appendix C, 1980, pp. C-1-C-13.

10 R.P. Koopman, R.T. Cederwall, D.L. Ermak, H.C. Godwire, Jr., W.J. Hogan, J.W. McClure, T.G. McRae, D.L. Morgan, H.C. Rodean and J.H. Shinn, Analysis of Burro series 40-m^3 LNG spill experiments, J. Hazardous Materials, 6 (1982) 43-83.

11 D.E. Neff and R.N. Meroney, The behavior of LNG vapor clouds: wind-tunnel simulation of 40 m^3 LNG spill tests at China Lake Naval Weapons Center, California, Gas Research Institute Report No. GRI 80/0094, Chicago, IL, 1981, 155 pp.

12 R.N. Meroney, Transient characteristics of dense gas dispersion. part I: A depth-averaged numerical model, J. Hazardous Materials, 9 (1984) 139-157.

13 R.N. Meroney, Quarterly report: test and design guidelines for fluid modeling of LNG vapor clouds, Gas Research Institute Contract No. 5083-252-0962, December-February, 1985, 10 pp.

14 R.G. Picknett, Dispersion of dense gas puffs released in the atmosphere at ground level, Atmos. Envir., 15 (1981) 509-525.

15 D.J. Hall, E.J. Hollis and H. Ishaq, A wind-tunnel model of the Porton dense gas spill field trials, Warren Springs Laboratory Report No. LR 394 (AP), Dept. of Trade and Industry, Stevenage, Hertfordshire, Great Britain, 1982, 103 pp.

16 A.C. Barrell and J. McQuaid, The HSE program of research and model development on heavy gas dispersion, I. Chem. Eng. Symposium on the Assessment and Control of Major Hazards, Manchester, Great Britain, April 22-24, 1985, 17 pp.

17 J. McQuaid, Overview of current state of knowledge on heavy gas dispersion and outstanding problems/issues, In: R.V. Portelli (Ed.), Proc. Heavy Gas (LNG/LPG) Workshop, Toronto, Ontario, January 29-30, 1985, pp. 5-28.

18 B. Roebuck, The presentation and availability of the data and plans for future analysis. In: J. McQuaid (Ed.), Heavy Gas Dispersion Trials at Thorney Island, J. Hazardous Materials, 11 (1985) 373-380

19 D.J. Hall and R.A. Waters, Wind-tunnel model comparisons with the Thorney Island dense gas release field trials, Warren Springs Laboratory Report LR 489 (AP)M, Dept. of Trade and Industry, Stevenage, Hertfordshire, Great Britain, 1985, 39 pp.

20 W.H.H. van Heugten and N.J. Duijm, Some findings based on wind tunnel simulation and model calculations of Thorney Island trial No. 008, In: J. McQuaid (Ed.), Heavy Gas Dispersion Trials at Thorney Island, J. Hazardous Materials, 11 (1985) 409-416.

21 N.J. Duijm, A.P. van Ulden and W.H.H. van Heugten, Physical and mathematical modeling of heavy gas dispersion - accuracy and reliability, 15th International Technical Meeting on Air Pollution Modelling and Its Applications, Washington University, St. Louis, April 16-19, 1985, 17 pp.

22 M. Schatzmann, G. Konig and A. Lohmeyer, Dispersion modeling of hazardous materials in the wind tunnel, 15th Int. Meeting on Air Pollution Modeling and Its Applications, April 15-18, 1985, St. Louis, MO, 12 pp.

23 D.E. Neff and R.N. Meroney, The behavior of LNG vapor clouds: Wind-tunnel tests on the modeling of heavy plume dispersion, Gas Research Institute Report No. GRI 80/0145, Chicago, IL, 1982, 120 pp.

24 G.W. Colenbrander and J.S. Puttock, Maplin Sands experiments 1980: interpretation and modeling of liquefied gas spills onto the sea, In: G. Ooms and H. Tennekes (Eds.), Atmospheric Dispersion of Heavy Gases and Small Particles, IUTAM Symposium on Delft 1983, Springer-Verlag, Berlin, 1984, pp. 277-295.

25 J.S. Puttock and G.W. Colenbrander, Dense gas dispersion - experimental research, In: R.V. Portelli (Ed.), Proc. Heavy Gas (LNG/LPG) Workshop, Toronto, Ontario, January 29-30, 1985, pp. 32-50.

26 G.W. Colenbrander and J.S. Puttock, personal communication, 1984.
27 K. Moodie, G. Taylor and H. Beckett, Water spray barrier trials: 181, Test parameters and concentration data for trials 35–48, Health and Safety Executive Report FM/15/82/3, Great Britain, 1981, 60 pp.
28 R.E. Britter, The spread of a negatively buoyant plume in a calm environment, Atmos. Envir., 13 (1979) 1241–1247.
29 R.N. Meroney, D.E. Neff and G. Heskestad, Wind-tunnel simulation of field dispersion tests (by the U.K. Health and Safety Executive) of water-spray curtains, Boundary-Layer Meteorol., 28 (1984) 107–119.
30 R.E. Britter, The ground level extent of a negatively buoyant plume in a turbulent boundary layer, Atmos. Envir., 14 (1980) 779–785.
31 S.T. Chan and D.L. Ermak, Recent progress in modeling the atmospheric dispersion of heavy gases over variable terrain using the three-dimensional conservation equations, IUTAM Symposium on Atmospheric Dispersion of Heavy Gases and Small Particles, Delft University of Technology, The Netherlands, August 29 – September 2, 1983, 32 pp.

Appendix A: Figs. A-1 – A-16

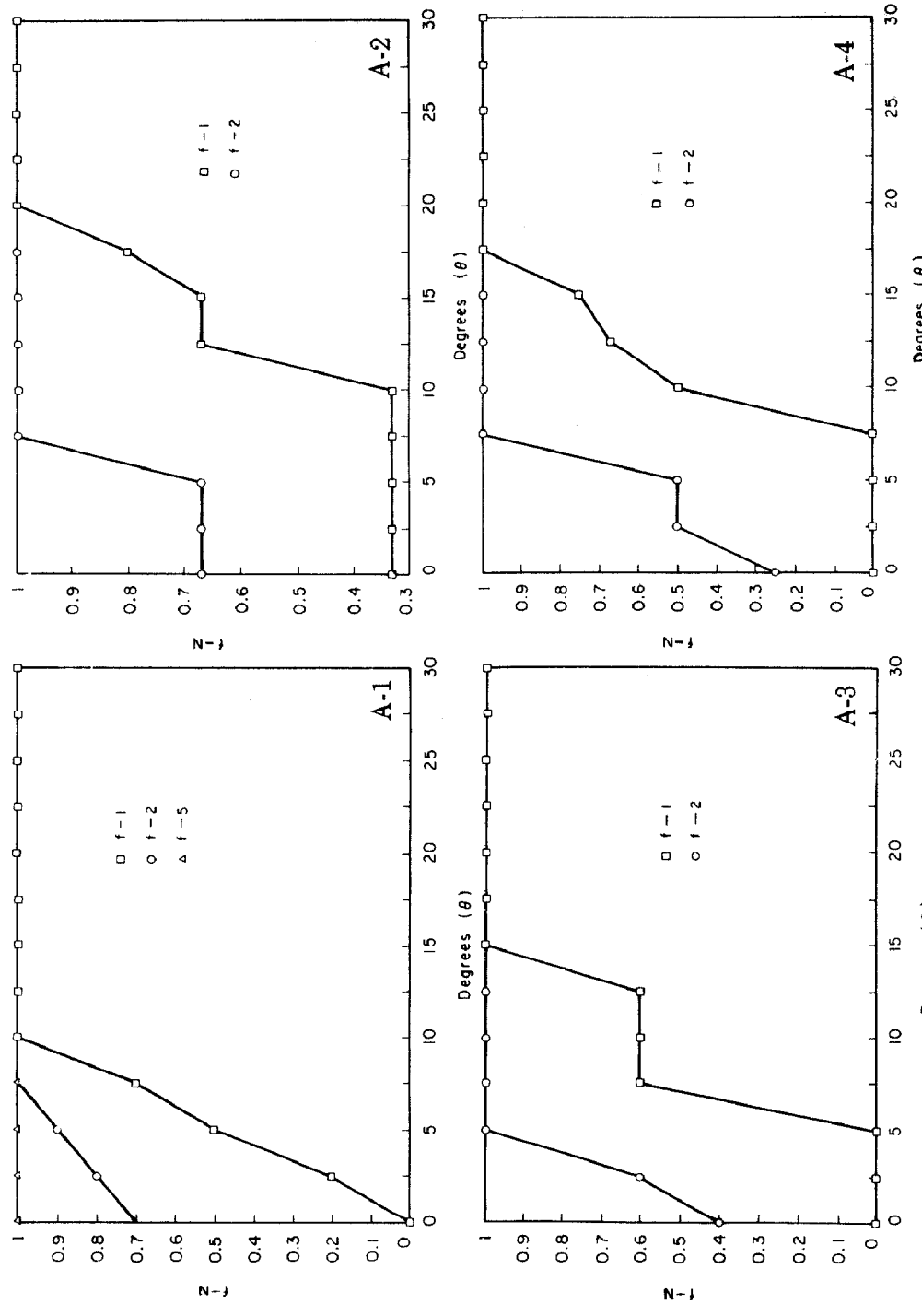

Fig. A-1. Capistrano test 44, case 11. Fig. A-2. China Lake 5 m^3 spills, LNG-18. Fig. A-3. China Lake 5 m^3 spills, LNG-19. Fig. A-4. China Lake 5 m^3 spills, LNG-20.

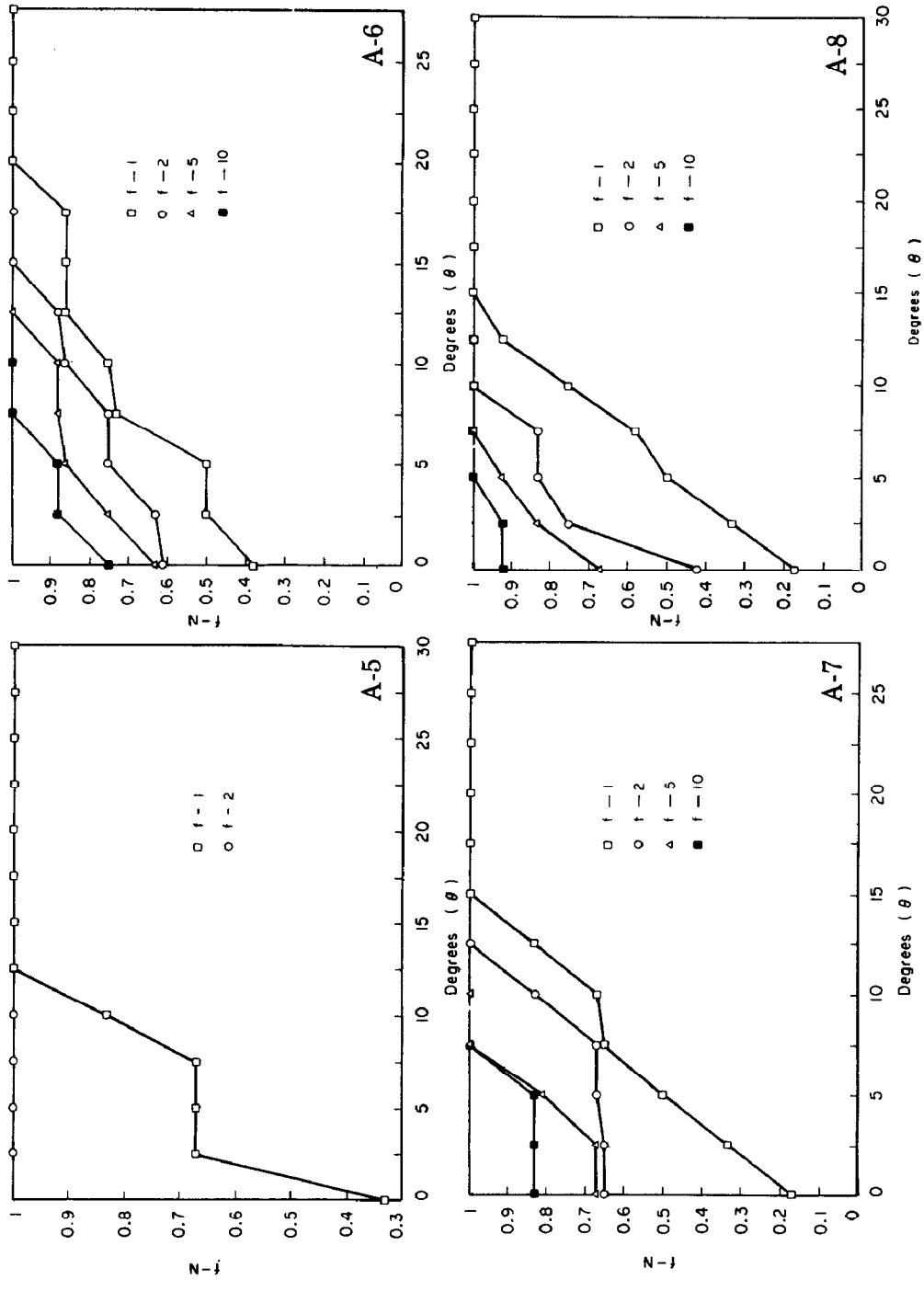

Fig. A-5. China Lake 5 m^3 spills, LNG-21. Fig. A-6. Burro No. 4. Fig. A-7. Burro No. 5. Fig. A-8. Burro No. 7.

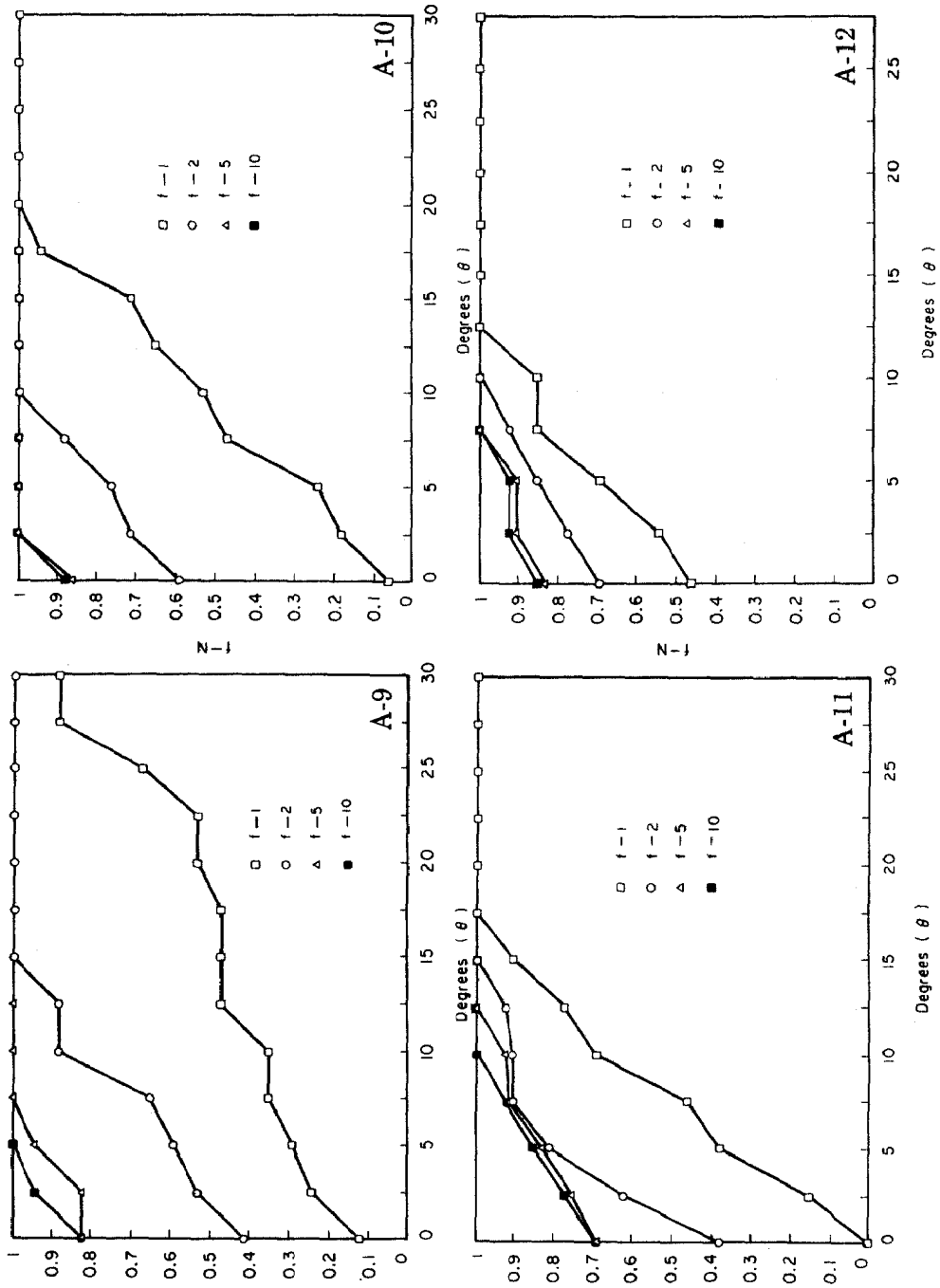

Fig. A-9. Burro No. 8 (1:85 scale, $S.G. = 1.38$). Fig. A-10. Burro No. 9 (1:240 model). Fig. A-11. Burro No. 8 (1:85 scale, $S.G. = 4.18$). Fig. A-12. Burro No. 9 (1:85 model).

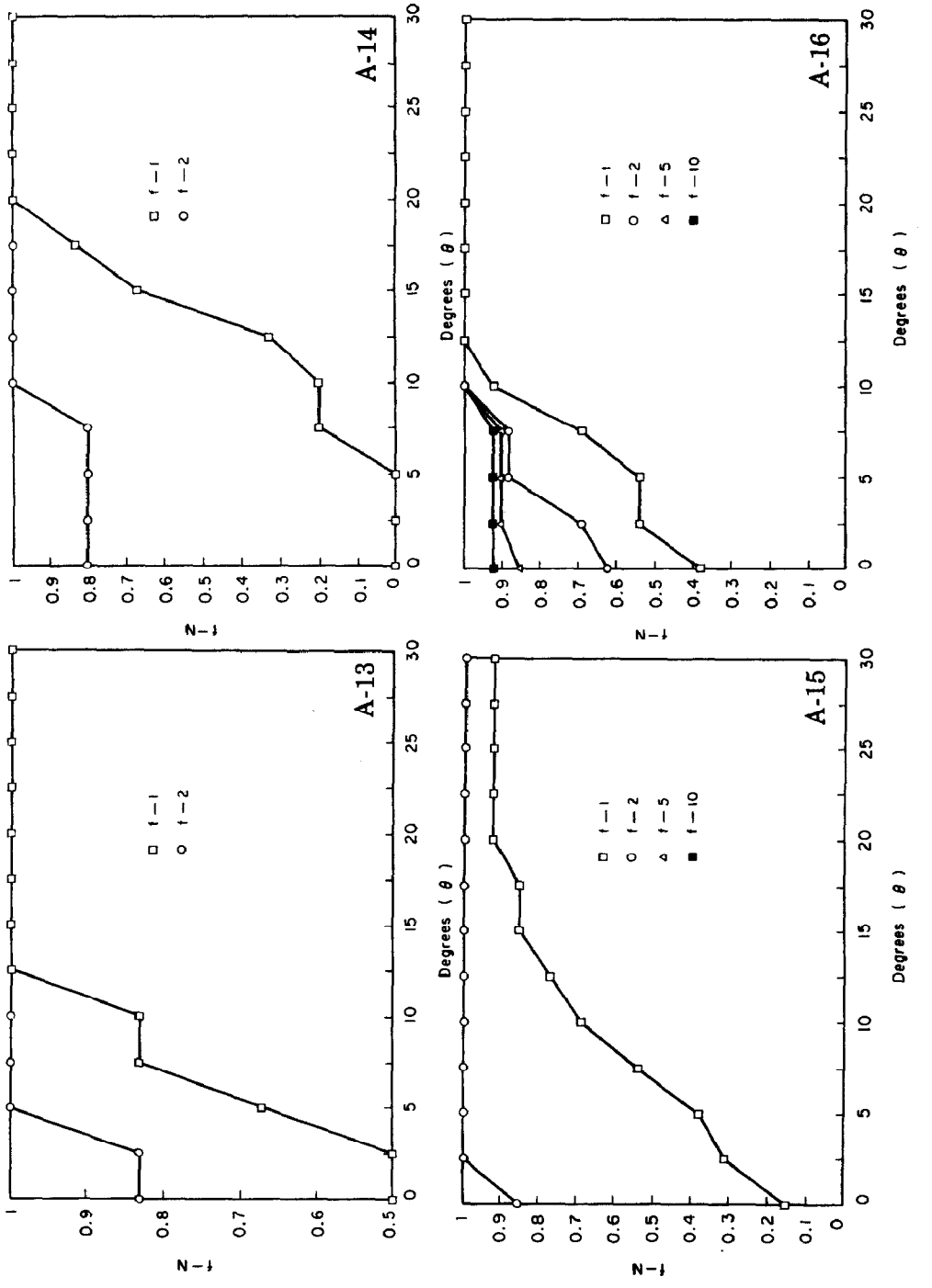

Fig. A-13. HSE run 46, spray. Fig. A-14. HSE run 46, no spray. Fig. A-15. Burro No. 8, FEM3 [31]. Fig. A-16. Burro No. 9, FEM3 [31].